

State estimation in wall-bounded flow systems. Part 2. Turbulent flows

By MATTIAS CHEVALIER^{1,2}, JÉRÔME HØPFFNER²,
THOMAS R. BEWLEY³ AND DAN S. HENNINGSON^{1,2}

¹The Swedish Defence Research Agency (FOI), SE-164 90, Stockholm, Sweden

²Department of Mechanics, Royal Institute of Technology, SE-100 44, Stockholm, Sweden

³Flow Control Lab, Department of MAE, UC San Diego, La Jolla, CA 92093, USA

(Received 16 November 2004 and in revised form 18 July 2005)

This work extends the estimator developed in Part 1 of this study to the problem of estimating a turbulent channel flow at $Re_\tau = 100$ based on a history of noisy measurements on the wall. The key advancement enabling this work is the development and implementation of an efficient technique to extract, from direct numerical simulations, the relevant statistics of an appropriately defined ‘external forcing’ term on the Navier–Stokes equation linearized about the mean turbulent flow profile. This forcing term is designed to account for the unmodelled (nonlinear) terms during the computation of the (linear) Kalman filter feedback gains in Fourier space. Upon inverse transform of the resulting feedback gains computed on an array of wavenumber pairs to physical space, we obtain, as in Part 1, effective and well-resolved feedback convolution kernels for the estimation problem. It is demonstrated that, by applying the feedback so determined, satisfactory correlation between the actual and estimated flow is obtained in the near-wall region. As anticipated, extended Kalman filters (with the nonlinearity of the actual system reintroduced into the estimator model after the feedback gains are determined) outperform standard (linear) Kalman filters on the full system.

1. Introduction

This paper builds directly on Part 1 of this study (Høpffner *et al.* 2005, hereafter referred to as Part 1). It extends the estimator developed there, for the case of perturbed laminar channel flow, to the problem of fully developed channel-flow turbulence. The reader is referred to Part 1 for related general references, background information on optimal state estimation (Kalman filter) theory, and a description of how to apply this theory to a well-resolved discretization of a fluid system in a manner that is consistent with the continuous PDE system upon which this discretization is based (that is, in a manner such that the resulting feedback convolution kernels converge upon refinement of the numerical grid).

The present paper effectively picks up where Part 1 left off, and treats specifically the issues involved in extending the estimator developed in Part 1 to the problem of estimating a fully developed turbulent channel flow based on wall measurements. Three key steps were identified in obtaining adequate estimator performance in the near-wall region:

(a) linearization of the flow system about the mean turbulent flow profile, accounting for the statistics of the additional forcing term during the computation of the feedback gains;

- (b) extraction of these statistics from a direct numerical simulation; and
- (c) incorporation of the nonlinearity of the actual system into the estimator model at the final step in the development of the estimator (using an extended Kalman filter).

Note also that the statistics of the forcing term used in the linear system description in this work are found to have some similarities to the parameterization of the external disturbances considered in Part 1, which dealt with the estimation of the early stages of transition in the same domain.

1.1. *Model predictive estimation*

There are two natural approaches for model-based estimation of near-wall turbulent flows: model predictive estimation and extended Kalman filtering. Bewley & Protas (2004) discusses the model predictive estimation approach, which is based on iterative state and adjoint calculations, optimizing the estimate of the state of the system such that the nonlinear evolution of the system model, over a finite horizon in time, matches the available measurements to the maximum extent possible. This is typically accomplished by optimizing the initial conditions in the estimator model in order to minimize a cost function measuring a mean-square ‘misfit’ of the measurements from the corresponding quantities in the estimator model over the time horizon of interest. This optimization is performed iteratively, using gradient information provided by calculation of an appropriately defined adjoint field driven by the measurement misfits at the wall. The technique provides an optimized estimate of the state of the system which accounts for the full nonlinear evolution of the system, albeit over a finite time horizon and providing only a local optimal which might be far from the actual flow state sought. The technique is typically expensive computationally, as it requires iterative marches of the state and adjoint fields over the time horizon of interest in order to obtain the state estimate; for this reason, this approach is often quickly disqualified from consideration as being computationally intractable for practical implementation. The model predictive estimation approach is closely related to the adjoint-based approach to weather forecasting, commonly known as 4D-var. For further discussion of model predictive estimation as it applies to near-wall turbulence, the reader is referred to Bewley & Protas (2004).

1.2. *Extended Kalman filtering*

The extended Kalman filter approach, which is the focus of the present paper, is described in detail in Part 1. To summarize it briefly, the estimation problem is first considered in the linearized setting. Define \hat{r} as the Fourier transform of the vector of all three measurements available on the walls in the actual flow system at wavenumber pair $\{k_x, k_z\}$, and define \check{r} as the corresponding quantity in the estimator model. At each wavenumber pair $\{k_x, k_z\}$, a set of feedback gains L is first computed such that a forcing term $\hat{v} = L(\hat{r} - \check{r})$ on the (linearized) estimator model results in a minimization of the energy of the estimation error (that is, this feedback minimizes the trace of the covariance of the estimation error, usually denoted P), assuming that the flow state itself is also governed by the same linearized model. This is called a Kalman filter, and the theory for the calculation of the optimal feedback gain L in the estimator is elegant, mathematically rigorous, and well known. For a comprehensive presentation in the ODE setting, see Anderson & Moore (1979). For the corresponding derivation in the spatially continuous (PDE) setting, see Balakrishnan (1976).

Upon inverse transform of the resulting feedback gains computed on an array of wavenumber pairs to physical space, we seek (and, indeed, find) well-resolved feedback

convolution kernels for the estimation problem that, far enough from the origin, decay exponentially with distance from the origin. The reader is referred to Bewley (2001), Bamieh, Paganini & Dahleh (2002), and Högberg, Bewley & Henningson (2003a) for further discussion of

(a) the technique used to transform feedback gains in Fourier space to feedback convolution kernels in physical space,

(b) an interpretation of what these convolution kernels mean in both the control and estimation problems, and

(c) a description of the overlapping decentralized control implementation facilitated by this approach, which is built from an interconnected array of identical tiles, each incorporating actuators, sensors, control logic, and limited communication with neighbouring tiles.

Ultimately, the estimator feedback \hat{v} is applied to a full (nonlinear) model of the flow system. This final step of reintroducing the nonlinearity of the system into the estimator model results in what is called an extended Kalman filter. In practice, the extended Kalman filter has proved to be one of the most reliable techniques available for estimating the evolution of nonlinear systems.

1.3. On the suitability of linear models of turbulence for state estimation and control

As described in the previous section, the feedback kernels used in the extended Kalman filter are calculated based on a linearized model of the fluid system. Thus, the applicability of the extended Kalman filtering strategy to turbulence is predicated upon the hypothesis that linearized models faithfully represent at least some of the important dynamic processes in turbulent flow systems.

The fluid dynamics literature of the last decade contains many articles aimed at supporting this hypothesis. For example, Farrell & Ioannou (1996) used these linearized equations in an attempt to explain the mechanism for the turbulence attenuation that is caused by the closed-loop control strategy now commonly known as opposition control. Jovanović & Bamieh (2001) proposed a stochastic disturbance model which, when used to force the linearized open-loop Navier–Stokes equation, led to a simulated flow state with certain second-order statistics (specifically, u_{rms} , v_{rms} , w_{rms} , and the Reynolds stress $-\overline{uv}$) that mimicked, with varying degrees of precision, the statistics from a full DNS of a turbulent flow at $Re_\tau = 180$.

Clearly, however, the hypothesis concerning the relevance of linearized models to the turbulence problem can only be taken so far, as linear models of fluid systems do not capture the nonlinear ‘scattering’ or ‘cascade’ of energy over a range of length scales and time scales, and thus linear models fail to capture an essential dynamical effect that endows turbulence with its inherent ‘multiscale’ characteristics. The key strategy of the present work (and, indeed, the key idea motivating our application of linear control theory to turbulence in general), is that the fidelity required of a model for it to be adequate for control (or estimator) design is in fact much lower than the fidelity required of a model for it to be adequate for accurate simulation of the system. Thus, for the purpose of computing feedback for the control and estimation problems, linear models might well be good enough, even though the fidelity of linear models as simulation tools to capture the open-loop statistics of turbulent flows is still the matter of some debate in the fluids literature. All that the feedback in an extended Kalman filter has to do is to give the estimator model a ‘nudge’ in approximately the right direction when the state and the state estimate are diverging. The extended Kalman filter contains the full nonlinear equations of the actual system in the estimator model, so if the state and the state estimate are sufficiently close, the

estimator will accurately track the state, for at least a short period of time, with little or no additional forcing necessary.

Put another way, in the control problem, the model upon which the control feedback is computed need only include the key terms responsible for the production of energy. As the nonlinear terms in the Navier–Stokes equation scatter energy but do not directly contribute to energy production, we might expect that a linear model may indeed suffice. For the control Navier–Stokes systems near solid walls based on full state information, Högberg, Bewley & Henningson (2003*b*) demonstrated complete relaminarization of low-Reynolds-number turbulent channel flow based on actuation at the wall using linear control theory, thereby providing compelling evidence that this is in fact true, at least for sufficiently low Reynolds number. The present work on the estimation problem is based on the related strategy that, in a similar manner, the model upon which the estimator feedback is computed might only need to capture the key terms responsible for the production of energy in the system describing the estimation error.

1.4. *The problem of nearly unobservable modes*

The problem of estimating the state of a chaotic nonlinear system based on limited noisy measurements of the system is inherently difficult. When posed as an optimization problem (for example, in the model predictive estimation approach described previously), one can expect that, in general, multiple local minima of such a non-convex optimization problem will exist, many of which will be associated with state estimates that are in fact poor. These difficulties are exacerbated in the case of the estimation of near-wall turbulence by the fact that turbulence is a multiscale phenomenon (that is, it is characterized by energetic motions over a broad range of length scales and time scales that interact in a nonlinear fashion), with significant nonlinear chaotic dynamics evolving far from where sensors are located (that is, on the walls).

As illustrated in figure 1(*b*) and table 1 of Bewley & Liu 1998 (hereafter, BL98) and discussed further in Part 1, even in the laminar case, at $k_x = 1$, $k_z = 0$ a significant number of the leading eigenmodes of the system are ‘centre modes’ with little support near the walls, and are thus nearly unobservable with wall-mounted sensors. As easily shown via similar plots in the turbulent case at the same and higher bulk Reynolds numbers, an even higher percentage of the leading eigenmodes of the linearized system are nearly unobservable in the turbulent case, with the problem getting worse as the Reynolds number is increased. We thus see that the problem of estimating turbulence is fundamentally harder than the problem of estimating perturbations to a laminar flow even if the linear model of turbulence is considered as valid, simply due to the heightened presence of nearly unobservable modes.

In the present work we focus our attention primarily on getting an accurate state estimate fairly close to the walls, where the sensors are located. This is done with the idea in mind that, in the problem of turbulence control (which is our ultimate long-term objective in this effort, and the reason we are pursuing this line of investigation), it is the near-wall region only that, on average, turbulence ‘production’ substantially exceeds ‘dissipation’, as pointed out in Jimenez (1999). Thus, we proceed with the objective that, if we can

- (a) estimate the fluctuations in the near-wall region with a sufficient degree of accuracy, then
- (b) subdue these near-wall fluctuations with appropriate control feedback,

then we will have a net stabilizing effect on the turbulent motions in the entire flow system, even if we do not completely relaminarize the turbulent flow. It is thus unnecessary to estimate accurately the motion of the flow far from the wall in order to realize our ultimate objective in this work. Such flow-field fluctuations, which will not be estimated accurately in this work, will (through nonlinear interactions) act as disturbances to excite continuously the state estimation error in the near-wall region, while feedback from the sensors will be used to subdue continuously this error.

The non-normality of the Orr–Sommerfeld/Squire operator in the laminar case is most evident by examining it near $k_x = 0$, $k_z = 2$, as illustrated in figure 2(b) of BL98 and quantified by the transfer function norms in table 4 of BL98. Similar plots reveal that the degree of non-normality of the eigenvectors (that is, the fact that, after the first, these eigenvectors come in pairs of almost exactly the same shape) is not significantly altered when moving from the laminar case to the turbulent case at the same bulk Reynolds number, though it is exacerbated gradually as the Reynolds number is increased. Note that, as opposed to the case at $k_x = 1$, $k_z = 0$ discussed above, all leading modes in the case $k_x = 0$, $k_z = 2$ have a substantial footprint on the wall. Thus, the situation is not as bad as it might first appear: even when linearized about the turbulent flow profile, at the wavenumbers of primary concern (in which the non-normality of the eigenmodes of the system matrix is most pronounced), these eigenmodes are easily detected by wall-mounted sensors. Further, the pairs of eigenmodes with nearly the same shape are easily distinguished during the dynamic state estimation process, as they are associated with different eigenvalues characterizing their variation in time.

1.5. Comparison of the estimation and control problems applied to near-wall turbulence

Another significant difference between the turbulence control and turbulence estimation problems is that, in the control problem, once (if) the control becomes effective, the system approaches a stationary state in which the linearization of the system is valid. In the estimation problem, on the other hand, even if the estimate at some time is quite accurate, the system is still moving on its chaotic attractor, so the linearization of the system about some mean state is not strictly valid. Thus, in this respect, it is seen that the turbulence estimation problem might be considered as being fundamentally harder than the turbulence control problem.

1.6. Outline

A brief review of the governing equations and some of the particular properties of the extended Kalman filter used in this work is given in §2. Section 3 collects and analyses the relevant statistics from a direct numerical simulation (DNS) of a turbulent channel flow at $Re_\tau = 100$ in order to build the estimator. The statistical data from §3 are then used in §4 to compute feedback gains (in Fourier space) and kernels (in physical space) for the estimator. The performance of the resulting estimator is evaluated via DNS in §5, and §6 presents some concluding remarks.

2. Governing equations

2.1. State equation and identification of terms lumped into the ‘external forcing’ f

The system model considered in this work is the Navier–Stokes equation for the three velocity components $\{U, V, W\}$ and pressure P of an incompressible channel flow, written as a (nonlinear) perturbation about a base flow profile $\bar{u}(y)$ and bulk pressure

variation $\bar{p}(x, y, t)$ such that, defining

$$\begin{pmatrix} U \\ V \\ W \\ P \end{pmatrix} = \begin{pmatrix} u \\ v \\ w \\ p \end{pmatrix} + \begin{pmatrix} \bar{u}(y) \\ 0 \\ 0 \\ \bar{p}(x, y, t) \end{pmatrix}$$

with $\{u, v, w, p\}$ varying in $\{x, y, z, t\}$ with periodic boundary conditions in the x - and z -directions, we have

$$\frac{\partial u}{\partial t} + \bar{u} \frac{\partial u}{\partial x} + v \frac{\partial \bar{u}}{\partial y} = -\frac{\partial p}{\partial x} + \frac{1}{Re} \Delta u + n_1, \tag{2.1a}$$

$$\frac{\partial v}{\partial t} + \bar{u} \frac{\partial v}{\partial x} = -\frac{\partial p}{\partial y} + \frac{1}{Re} \Delta v + n_2, \tag{2.1b}$$

$$\frac{\partial w}{\partial t} + \bar{u} \frac{\partial w}{\partial x} = -\frac{\partial p}{\partial z} + \frac{1}{Re} \Delta w + n_3, \tag{2.1c}$$

$$\frac{\partial u}{\partial x} + \frac{\partial v}{\partial y} + \frac{\partial w}{\partial z} = 0, \tag{2.2}$$

where

$$\left. \begin{aligned} n_1 &= -u \frac{\partial u}{\partial x} - v \frac{\partial u}{\partial y} - w \frac{\partial u}{\partial z} - \frac{\partial \bar{p}}{\partial x} + \frac{1}{Re} \frac{\partial^2 \bar{u}}{\partial y^2}, \\ n_2 &= -u \frac{\partial v}{\partial x} - v \frac{\partial v}{\partial y} - w \frac{\partial v}{\partial z} - \frac{\partial \bar{p}}{\partial y}, \\ n_3 &= -u \frac{\partial w}{\partial x} - v \frac{\partial w}{\partial y} - w \frac{\partial w}{\partial z}. \end{aligned} \right\} \tag{2.3}$$

We select the base flow profile $\bar{u}(y)$ as the average in $x, z,$ and t of the turbulent flow,

$$\bar{u}(y) = \lim_{T \rightarrow \infty} \frac{1}{T L_x L_z} \int_0^T \int_0^{L_x} \int_0^{L_z} U \, dz \, dx \, dt,$$

and the variation of $\bar{p}(x, y, t)$ in the x -direction as the (unsteady) mean pressure gradient sustaining the flow with a constant mass flux in the streamwise direction. Note that the (steady) variation of $\bar{p}(x, y, t)$ in the y -direction arises to balance the average in $x, z,$ and t of the $v \partial v / \partial y$ term in the wall-normal momentum equation. Note also that we assume no-slip solid walls ($U = V = W = u = v = w = 0$ on $y = \pm 1$). This facilitates decomposition of the perturbation problem (2.1) in the x - and z -directions using a Fourier series.

We now apply such a Fourier decomposition to (2.1), using hat subscripts ($\hat{\cdot}$) to denote the Fourier representation. The system may then be transformed to $\{\hat{v}, \hat{\eta}\}$ form in a straightforward fashion. Applying the Laplacian $\Delta = \partial^2 / \partial y^2 - k^2$, where $k^2 = k_x^2 + k_z^2$, to the Fourier transform of (2.1b), substituting for $\Delta \hat{p}$ from the divergence of the Fourier transform of (2.1), and applying the Fourier transform of (2.2) gives the equation for \hat{v} . Subtracting ik_x times the Fourier transform of (2.1c) from ik_z times the Fourier transform (2.1a) gives the equation for $\hat{\eta} = ik_z \hat{u} - ik_x \hat{w}$. The result is the linear Orr–Sommerfeld/Squire equations at each wavenumber pair $\{k_x, k_z\}$ with an extra term accounting for the nonlinearity of the system

$$\frac{d}{dt} M \hat{q} + L \hat{q} = T \hat{n} \tag{2.4}$$

where

$$\hat{q} = \begin{pmatrix} \hat{v} \\ \hat{\eta} \end{pmatrix}, \quad \hat{n} = \begin{pmatrix} \hat{n}_1 \\ \hat{n}_2 \\ \hat{n}_3 \end{pmatrix}, \quad M = \begin{pmatrix} -\Delta & 0 \\ 0 & I \end{pmatrix}, \quad L = \begin{pmatrix} \mathcal{L} & 0 \\ \mathcal{C} & \mathcal{S} \end{pmatrix}, \quad T = \begin{pmatrix} ik_x D & k^2 & ik_z D \\ ik_z & 0 & -ik_x \end{pmatrix},$$

and

$$\begin{aligned} \mathcal{L} &= -ik_x \bar{u} \Delta + ik_x \bar{u}'' + \Delta^2 / Re, \\ \mathcal{S} &= ik_x \bar{u} - \Delta / Re, \\ \mathcal{C} &= ik_z \bar{u}', \end{aligned}$$

where $\{\hat{n}_1, \hat{n}_2, \hat{n}_3\}$ are given by the Fourier transform of (2.3), taking (from the Fourier transform of (2.2) and the definition of $\hat{\eta}$)

$$\hat{u} = \frac{i}{k^2} \left(k_x \frac{\partial \hat{v}}{\partial y} - k_z \hat{\eta} \right), \quad \hat{w} = \frac{i}{k^2} \left(k_z \frac{\partial \hat{v}}{\partial y} + k_x \hat{\eta} \right),$$

and where, with the walls located at $y = \pm 1$ and the velocities normalized such that the peak value of $\bar{u}(y)$ is 1, Re is the Reynolds number based on the centreline velocity and channel half-width. Note that, for $k_x = k_z = 0$, it follows immediately from the definition of this system that $\hat{v} = \hat{\eta} = 0$ for all y . For all other wavenumber pairs, multiplying (2.4) by M^{-1} , we obtain

$$\dot{\hat{q}} = \underbrace{-M^{-1}L}_A \hat{q} + \underbrace{M^{-1}T}_B \hat{n}. \quad (2.5)$$

Note that the terms in this expression depend on the wavenumber pair being considered, $\{k_x, k_z\}$, and that the state \hat{q} is a continuous function of both the wall-normal coordinate y and the time coordinate t . Implementation of this equation in the computer requires discretization of this system in the wall-normal direction y and a discrete march in time t .

The present system may be linearized by replacing the exact expression for n by an appropriate stochastic model, which we will denote f , thereby obtaining the linear state-space model

$$\dot{\hat{q}} = A\hat{q} + B\hat{f}. \quad (2.6)$$

As the mean of n is everywhere zero, it is logical to select this stochastic model such that $E[f] = 0$, where the expectation operator $E[\cdot]$ is defined as the average over many realizations of the stochastic quantity in brackets. The covariance of f will be modelled carefully based on the covariance of n observed in DNS, as discussed further in §2.3.

2.2. Measurements

The present work attempts to develop the best possible estimate of the state based on measurements of the flow on the walls. As discussed in Part 1, and in greater detail in Bewley & Protas (2004), the three independent measurements available on the walls are the distributions of the streamwise and spanwise wall skin friction and the wall pressure.

In the present paper, we have chosen to transform these measurements to a slightly different form such that their effects on the estimation of the system (2.6), which is in $\{\hat{v}, \hat{\eta}\}$ form, is more transparent. There is some flexibility here; in the present work, we have chosen to define this transformed measurement vector \hat{f} to contain scaled

versions of the wall values of the wall-normal derivative of the wall-normal vorticity, $\hat{\eta}_y/Re$, the second wall-normal derivative of the wall-normal velocity, \hat{v}_{yy}/Re , and the pressure, \hat{p} . Note that we can easily relate this transformed measurement vector to the raw measurements of $\hat{\tau}_x = D\hat{u}/Re$, $\hat{\tau}_z = D\hat{w}/Re$, and \hat{p} on the walls, which might be available from a lab experiment, via the relation (in Fourier space)

$$\hat{r} \triangleq \begin{pmatrix} \frac{1}{Re} \hat{\eta}_y|_{wall} \\ \frac{1}{Re} \hat{v}_{yy}|_{wall} \\ \hat{p}|_{wall} \end{pmatrix} = \underbrace{\begin{pmatrix} ik_z & -ik_x & 0 \\ -ik_x & -ik_z & 0 \\ 0 & 0 & I \end{pmatrix}}_K \begin{pmatrix} \hat{\tau}_x|_{wall} \\ \hat{\tau}_z|_{wall} \\ \hat{p}|_{wall} \end{pmatrix}, \quad (2.7)$$

and we may relate the transformed measurement vector \hat{r} to the state \hat{q} via the simple relation

$$\hat{r} = C\hat{q} + \hat{g} \quad \text{with} \quad C = \frac{1}{Re} \begin{pmatrix} 0 & D|_{wall} \\ D^2|_{wall} & 0 \\ \frac{1}{k^2} D^3|_{wall} & 0 \end{pmatrix}, \quad (2.8)$$

where \hat{g} accounts for the measurement noise. The last row of the above relation is easily verified by taking $\partial/\partial x$ of the x -momentum equation plus $\partial/\partial z$ of the z -momentum equation, then applying continuity and the boundary conditions.

For the purpose of posing the present state estimation problem, the measurements are assumed to be corrupted by uncorrelated zero-mean white Gaussian noise processes, which are assembled into the vector \hat{g} with an assumed covariance (in Fourier space) of

$$G = \begin{pmatrix} \alpha_\eta^2 & 0 & 0 \\ 0 & \alpha_v^2 & 0 \\ 0 & 0 & \alpha_p^2 \end{pmatrix}. \quad (2.9)$$

Note that such an assumption of uncorrelated white (in space and time) noise is in fact a fairly realistic model for electrical noise in the sensors. The role of G in tuning the strength of the estimator feedback is discussed in greater detail in Part 1.

A different parameterization for the noise covariance that might be of interest in a practical implementation, in which the physical sensors measure $\hat{\tau}_x$, $\hat{\tau}_y$, and \hat{p} , is

$$G = K \begin{pmatrix} \alpha_{\tau_x}^2 & 0 & 0 \\ 0 & \alpha_{\tau_y}^2 & 0 \\ 0 & 0 & \alpha_p^2 \end{pmatrix} K^*, \quad (2.10)$$

where K is defined in (2.7) and the convenient relation given in (2.5) of Part 1 has been used to relate the covariance of the noise on the raw measurements to the present formulation. This parameterization should also be explored numerically in future work.

2.3. Extracting the relevant statistics for state estimation from resolved simulations

The performance of the estimator may be tuned by accurate parameterization of the relevant statistical properties of the forcing term f in the linearized state model, in addition to adjusting the parameterization of the statistical properties of the measurement noise \hat{g} . These statistics play an essential role in the computation of the Kalman filter feedback gains.

In the present work, we will assume that f is effectively uncorrelated from one time step to the next (that is, we assume that f is ‘white’ in time) in order to simplify the design of the estimator. Subject to this central assumption, we proceed by developing an accurate model for the assumed spatial correlations of f . As the system under consideration is statistically homogeneous in the x - and z -directions, the covariance of the stochastic forcing f may be parameterized in physical space as

$$E[f_j(x, y, z, t)f_k(x + r_x, y', z + r_z, t')] = \delta(t - t')\mathcal{Q}_{f_j f_k}(y, y', r_x, r_z),$$

where $\delta(t)$ denotes the Dirac delta and where the covariance $\mathcal{Q}_{f_j f_k}$ is determined by calculating the statistics of the actual nonlinear forcing term n in a DNS,

$$\mathcal{Q}_{f_j f_k}(y, y', r_x, r_z) = \lim_{T \rightarrow \infty} \frac{1}{T L_x L_z} \int_0^T \int_0^{L_x} \int_0^{L_z} n_j(x, y, z)n_k(x + r_x, y', z + r_z) dz dx dt. \quad (2.11)$$

As the system under consideration is statistically homogeneous, or ‘spatially invariant’, in the x - and z -directions, it is more convenient to work with the Fourier transform of the two-point correlation $\mathcal{Q}_{f_j f_k}$ rather than working with $\mathcal{Q}_{f_j f_k}$ itself, as the calculation of $\mathcal{Q}_{f_j f_k}$ in physical space involves a convolution sum, which reduces to a simple multiplication in Fourier space. The Fourier transform of $\mathcal{Q}_{f_j f_k}$, which we identify as the spectral density function $R_{\hat{f}_j \hat{f}_k}$, is defined as

$$R_{\hat{f}_j \hat{f}_k}(y, y', k_x, k_z) = \frac{1}{4\pi} \int_0^{L_x} \int_0^{L_z} \mathcal{Q}_{f_j f_k}(y, y', r_x, r_z) e^{-ik_x r_x - ik_z r_z} dr_x dr_z. \quad (2.12)$$

Note that, due to the statistical homogeneity of the system in x and z , the spectral density function $R_{\hat{f}_j \hat{f}_k}$ is a decoupled at each wavenumber pair $\{k_x, k_z\}$, and thus may be determined from the DNS according to

$$R_{\hat{f}_j \hat{f}_k}(y, y', k_x, k_z) = \lim_{T \rightarrow \infty} \frac{1}{T} \int_0^T \hat{n}_j(y, k_x, k_z) \hat{n}_k^*(y', k_x, k_z) dt. \quad (2.13)$$

Certain symmetries may be applied to accelerate the convergence of the statistics determined from the DNS and to reduce the amount of covariance data that needs to be stored, which is in fact quite large. Since $\mathcal{Q}_{f_j f_k}$ is a real-valued function, $R_{\hat{f}_j \hat{f}_k}$ is Hermitian, so

$$R_{\hat{f}_j \hat{f}_k}(y, y', k_x, k_z) = R_{\hat{f}_j \hat{f}_k}^*(y, y', -k_x, -k_z). \quad (2.14)$$

By (2.13), it follows immediately that

$$R_{\hat{f}_j \hat{f}_k}(y, y', k_x, k_z) = R_{\hat{f}_k \hat{f}_j}^*(y, y, k_x, k_z). \quad (2.15)$$

Due to the up/down and left/right statistical symmetry in the flow, it also follows that

$$R_{\hat{f}_j \hat{f}_k}(y, y', k_x, k_z) = \pm R_{\hat{f}_j \hat{f}_k}^*(-y, -y', k_x, k_z), \quad (2.16a)$$

$$R_{\hat{f}_j \hat{f}_k}(y, y', k_x, k_z) = \pm R_{\hat{f}_j \hat{f}_k}^*(y, y', k_x, -k_z), \quad (2.16b)$$

$$R_{\hat{f}_1 \hat{f}_3}(y, y', k_x, k_z) = R_{\hat{f}_2 \hat{f}_3}(y, y', k_x, k_z) = 0, \quad (2.16c)$$

where, in (2.16a), the minus sign is used for the cases $\{j = 2, k \neq 2\}$ and $\{j \neq 2, k = 2\}$, and the positive sign is used for all other cases and, in (2.16b), the minus sign is used for the cases $\{j = 3, k \neq 3\}$ and $\{j \neq 3, k = 3\}$, and the positive sign is used for all other cases. The reader is referred to, e.g., Moin & Moser (1989) for similar

computations. Finally, for later use, the individual components of the spectral density function $R_{\hat{f}\hat{f}}$ at each wavenumber pair $\{k_x, k_z\}$ are denoted by

$$R_{\hat{f}\hat{f}}(y, y', k_x, k_z) = \begin{pmatrix} R_{\hat{f}_1\hat{f}_1} & R_{\hat{f}_1\hat{f}_2} & R_{\hat{f}_1\hat{f}_3} \\ R_{\hat{f}_2\hat{f}_1} & R_{\hat{f}_2\hat{f}_2} & R_{\hat{f}_2\hat{f}_3} \\ R_{\hat{f}_3\hat{f}_1} & R_{\hat{f}_3\hat{f}_2} & R_{\hat{f}_3\hat{f}_3} \end{pmatrix}.$$

3. Statistics of the nonlinear term n

We now perform a DNS of the nonlinear Navier–Stokes equations in a turbulent channel flow at $Re_\tau = 100$, gathering the statistics of the nonlinear term n identified in (2.3), which combines all those terms which will be supplanted by the stochastic forcing f in the linearized model (2.6) upon which the Kalman filter will be based. Note that the Reynolds number $Re_\tau = u_\tau\delta/\nu$ is based on the mean skin friction velocity u_τ , the channel half-width δ , and the kinematic viscosity ν ; $Re_\tau = 100$ corresponds to $Re_{cl} = u_{cl}\delta/\nu = 1712$, where u_{cl} is the mean centreline velocity.

All DNS calculations performed in this work used the code of Bewley, Moin & Temam (2001). For the spatial discretization, this code uses dealiased pseudospectral techniques in the streamwise and spanwise directions and an energy-conserving second-order finite difference technique in the wall-normal direction. For the time march, the code uses a fractional step implementation of a hybrid second-order Crank–Nicolson/third-order Runge–Kutta–Wray method. The overall pressure gradient is adjusted at each time step in order to maintain a constant mass flux in the flow, and a computational domain of size $4\pi \times 2 \times 4\pi/3$ in the $x \times y \times z$ directions is used. The resolution is $42 \times 64 \times 42$ Fourier, finite difference, Fourier modes (that is, $64 \times 64 \times 64$ dealiased collocation points). The numerical scheme used to discretize the Orr–Sommerfeld/Squire equations in this work is the spectral Differentiation Matrix Suite of Weideman & Reddy (2000); for further discussion of this discretization, see Högberg *et al.* (2003a).

The covariance of the forcing term $n = (n_1, n_2, n_3)^T$ identified in (2.3) was sampled during a DNS long enough to obtain statistical convergence. During the simulation, the full covariance matrices were computed at each wavenumber pair, creating a large, four-dimensional data set. The size of the covariance data set is $N_x \times N_z \times N_y^2$ for each correlation component of the forcing vector (before exploiting any symmetries), where N_x , N_y , and N_z denote the resolution in the corresponding directions[†]. The symmetries mentioned in §2.3 were then applied in post-processing to improve the statistical convergence. These statistics are subsequently used in §4, where the optimal estimation feedback gains are computed. In §5, the feedback gains so determined are used in order to estimate a fully developed turbulent flow based on wall measurements alone. Both Kalman filters and extended Kalman filters are investigated.

In figure 1 the magnitude of the spectral density function at four representative wavenumber pairs $\{k_x, k_z\}$ is plotted. As seen in the figure (plotted along the main diagonal), the variance of the forcing terms is stronger in the high-shear regions near the walls, as expected. Note also that there is a pronounced cross-correlation between

[†] As resolution requirements of turbulence simulations increase quickly with increasing Reynolds number, at higher Reynolds numbers (to be explored in future work) it will thus be necessary to represent only the most significant components of these correlations via an approximate strategy, accounting only for the leading singular values of these correlation matrices at each wavenumber pair.

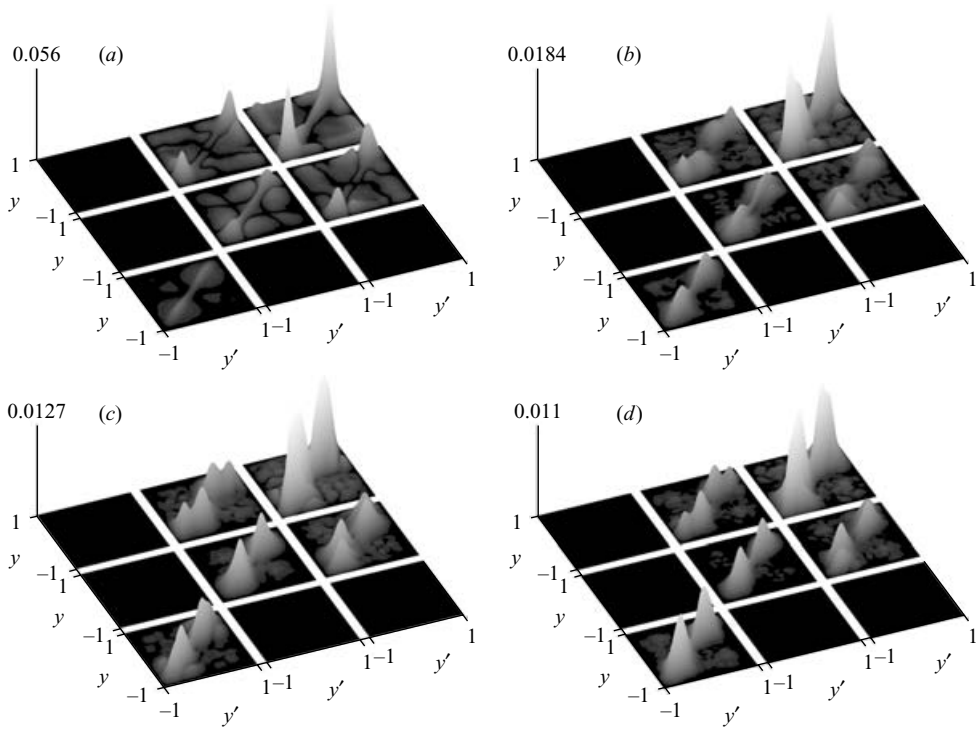


FIGURE 1. The magnitude of the spectral density function $R_{\hat{f}\hat{f}}(y, y', k_x, k_z)$ of \hat{f} , computed from the DNS of a turbulent channel flow at $Re_\tau = 100$, at wavenumber pairs $\{k_x, k_z\}$ of (a) $\{1.0, 3.0\}$, (b) $\{3.0, 1.5\}$, (c) $\{0.0, 1.5\}$, and (d) $\{4.0, 4.5\}$. The nine ‘squares’ correspond to the correlation between the various components of the forcing vector; from furthest to the viewer to closest to the viewer, the squares correspond to the \hat{f}_1 , \hat{f}_2 , and \hat{f}_3 components on each axis. The width of each side of each square represents the width of the channel, $[-1, 1]$. The variance is plotted along the diagonal of each square.

f_1 and f_2 , accounting for the Reynolds stresses in the flow, with the other cross-correlations converging towards zero as the statistical basis is increased. Figure 3(a) shows the corresponding variation of the maximum magnitude of the spectral density function as a function of the wavenumbers k_x and k_z . As expected, the stochastic forcing is stronger for lower wavenumber pairs.

In figure 2, a corresponding plot of the magnitude of the spectral density function of the stochastic forcing model defined in Part 1 is given. Note that the shape of this covariance model is invariant with $\{k_x, k_z\}$. It is only the overall magnitude of this covariance model that varies with $\{k_x, k_z\}$, in contrast to the covariance data determined from the DNS data, as reported in figure 1. Figure 3(b) shows the corresponding variation of the maximum magnitude of the spectral density function as a function of the wavenumbers k_x and k_z .

4. Estimator gains and the corresponding physical-space kernels

In Högberg *et al.* (2003a), the covariance Q was modelled with a spatially uncorrelated stochastic forcing, $Q = I$. With that model, it proved to be impossible to obtain well-resolved estimation gains for more than one measurement (of η_y), essentially because the problem defined did not converge as the grid was refined.

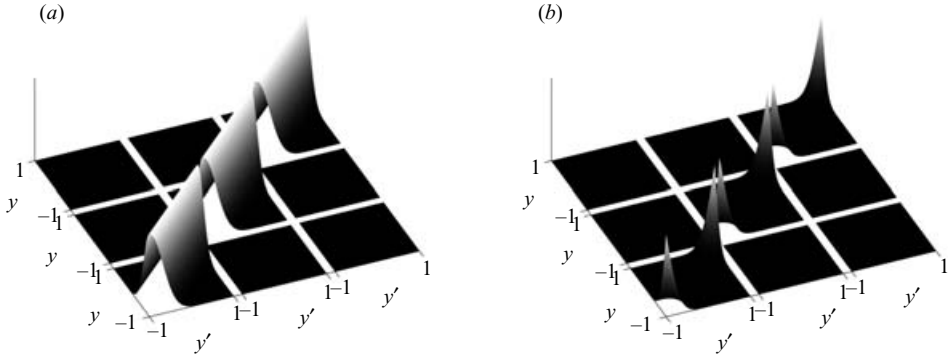


FIGURE 2. The magnitude of the spectral density function $R_{\hat{f}\hat{f}}(y, y', k_x, k_z)$ of \hat{f} , as parameterized in the laminar model proposed in Part 1, taking $p = 0$ (a) and $p = 3$ (b); see figure 1 for further explanation of the plot.

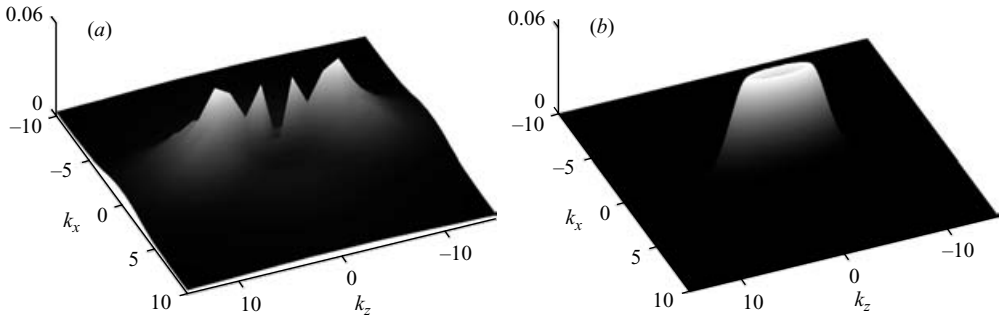


FIGURE 3. The variation of the maximum amplitude of the spectral density function as a function of the wavenumbers k_x and k_z for the DNS data of \hat{f}_1 (a) and the statistical model of Part 1 (b).

Part 1 of this study fixed this problem, where it was shown that, using appropriately smooth models for the covariance functions, well-resolved estimation kernels could be obtained for all three measurements available at the wall (specifically, η_y and v_{yy} (equivalently, τ_x and τ_z) and p). The present study takes this approach one step further, obtaining the covariance of the stochastic forcing terms directly from data obtained via DNS. Basing the stochastic model on the turbulent statistics, we again obtain well-resolved gains that converge upon grid refinement for all three measurements available at the wall. The definition and solution procedure for the state estimation problem in order to solve for the Kalman filter gains in the estimator in the present work are identical to that described in Part 1, to which the reader is referred for further details.

Figure 4 illustrates isosurfaces of the physical-space convolution kernels based on the statistics of the neglected terms in the linearized model, as determined from DNS. (Note that these gains are transformed to gains based on η_y , v_{yy} , and p in the estimator simulations presented in § 5.) The kernels depicted in figure 4 are substantially different in shape from those used in the laminar case, as reported in figure 12 of Part 1; in particular, note that they are generally more focused in the region adjacent to the lower wall, probably as consequence of the fuller mean velocity profile about which the system is linearized in the turbulent case.

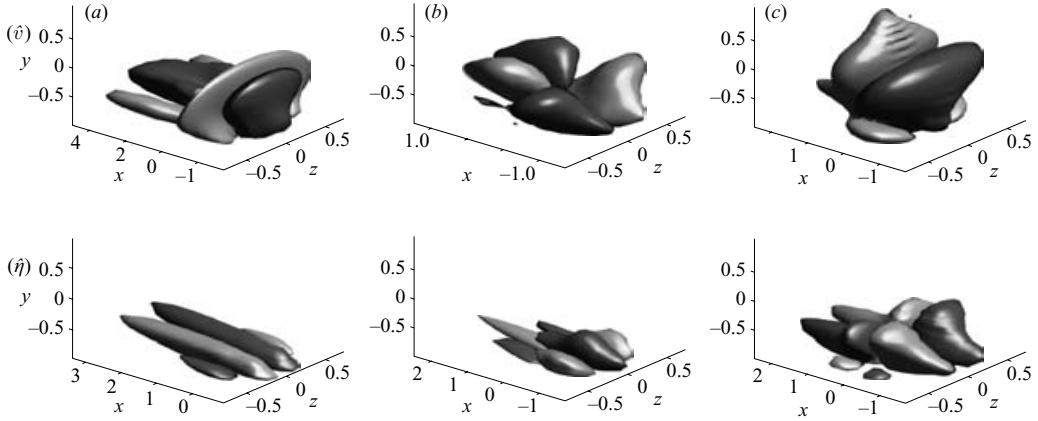


FIGURE 4. Isosurfaces of the physical-space convolution kernels determined for $Re_\tau = 100$ turbulent channel flow based on the statistics of the neglected terms in the linearized model, as determined by DNS and plotted in figures 1 and 3(a). Shown are the steady-state convolution kernels relating the (a) τ_x , (b) τ_z , and (c) p measurements at the point $\{x = 0, y = -1, z = 0\}$ on the wall to the estimator forcing on the interior of the domain for the evolution equation for the estimate of (top) v and (bottom) η . Visualized are positive (dark) and negative (light) isosurfaces with isovalues of $\pm 5\%$ of the maximum amplitude for each kernel illustrated.

| Case | α_η | α_v | α_p | Q | $J^{1/2}$ |
|------|---------------|------------|------------|----------------------|-----------|
| 1 | 0.1200 | – | – | I | 52 |
| 2 | 0.0037 | – | – | $R_{\hat{f}\hat{f}}$ | 52 |
| 3 | 0.0030 | 0.0030 | – | $R_{\hat{f}\hat{f}}$ | 55 |
| 4 | 0.0030 | 0.0030 | 0.0075 | $R_{\hat{f}\hat{f}}$ | 53 |

TABLE 1. The estimation simulations. For the cases when using one and two measurements, only the corresponding α values are relevant since the other measurements are excluded from the C -matrix.

The level of the sensor noise, described in §2.2, is a natural ‘knob’ to tune the magnitude of the contribution to the estimator feedback from each of the individual measurements. In an attempt to make a reasonably fair comparison between the different stochastic models, we define measures of the η_y kernel

$$J = \int_{-1}^1 \int_0^{L_x} \int_0^{L_z} L_{\eta_y}^2 \, dx \, dy \, dz.$$

Such a quantity measures the integral in all three spatial directions of the square of the gain corresponding to the η_y measurement.

Four cases were studied, as shown in table 1. In all four cases, the relevant α parameters were tuned so that the sum J of the measure η_y is approximately equal. The logic for performing the comparison in this way is to study the additional information provided when the additional measurements are added while the covariance of the system is accurately modelled. Future studies should experiment with tuning the relevant α parameters differently (corresponding to changing the relative noise on each of the three types of sensors) in order to find the most effective combination. Note that, with the current choice of the α parameters, the addition of the feedback

into the estimator required no adjustment of the time step for the extended Kalman filter DNS to run properly.

5. Estimator performance

5.1. Estimator algorithm

In order to quantify the performance of the Kalman filter developed in this work, we run two direct numerical simulations in parallel. One simulation represents the ‘real’ flow, where the initial condition is a fully developed turbulent flow field. The other simulation represents the estimated flow field, and is initialized with a turbulent mean flow profile and all fluctuating velocity components set to zero. The real flow is modelled by the Navier–Stokes equation. In the estimator simulations we have tested both Kalman filters (with the state model being the linearized Navier–Stokes equation) and extended Kalman filters (with the state model being the full nonlinear Navier–Stokes equation).

In the estimator simulations the volume forcing v , defined in §1.2, is added. This additional forcing is based on the wall measurements and the precomputed estimation gains L . For the Kalman filter simulations, we fix the mean flow to the turbulent mean flow profile and compute the velocity fluctuations using the linearized Navier–Stokes equation.

To evaluate the performance of the Kalman and extended Kalman filters, the *correlation* between the actual and estimated flow is defined throughout the wall-normal extent of the domain at each instant of time according to

$$\text{corr}_y(s, \check{s}) = \frac{\int_0^{L_x} \int_0^{L_z} s \check{s} \, dx \, dz}{\left(\int_0^{L_x} \int_0^{L_z} s^2 \, dx \, dz \right)^{1/2} \left(\int_0^{L_x} \int_0^{L_z} \check{s}^2 \, dx \, dz \right)^{1/2}}, \quad (5.1)$$

where s and \check{s} represent either a velocity component, or the pressure, or the Reynolds stresses from the actual and estimated flow, respectively. A correlation of 1 means perfect correlation whereas correlation zero means no correlation at all. Another useful quantity to study is the *error* between the actual and estimated flow state, defined as

$$\text{err}_y(s, \check{s}) = \frac{\left(\int_0^{L_x} \int_0^{L_z} (s - \check{s})^2 \, dx \, dz \right)^{1/2}}{\left(\int_0^{L_x} \int_0^{L_z} s^2 \, dx \, dz \right)^{1/2}}. \quad (5.2)$$

The error (5.2) ranges from zero, which means no error between the real and estimated flow fields, to infinity. Finally, perhaps the most pertinent quantity to measure is the kinetic energy of the *total error* between the real and estimated velocity fields, defined (with \mathcal{Q} selected appropriately, as required to measure the energy of the velocity field) as

$$\text{err}_y^{\text{tot}}(q, \check{q}) = \frac{\left(\int_0^{L_x} \int_0^{L_z} (q - \check{q})^* \mathcal{Q} (q - \check{q}) \, dx \, dz \right)^{1/2}}{\left(\int_0^{L_x} \int_0^{L_z} q^* \mathcal{Q} q \, dx \, dz \right)^{1/2}}. \quad (5.3)$$

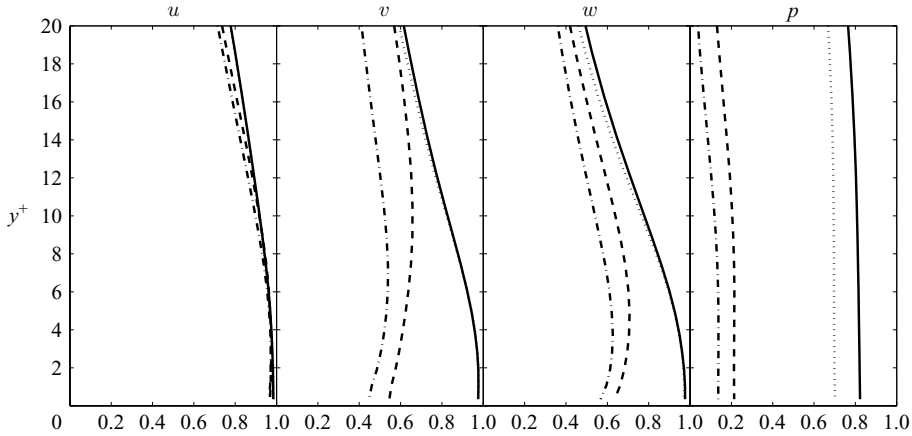


FIGURE 5. $\text{corr}_y(s, \hat{s})$ for $s = u$, $s = v$, $s = w$, and p obtained using the Kalman filter. The solid line denotes estimation using all three measurements and noise statistics as discussed in § 3. The dashed line denotes the estimator performance using only the η_y measurement. The dash-dotted line is obtained using the spatially uncorrelated stochastic model for noise statistics. The dotted line denotes the estimator performance using the η_y and v_{yy} measurements.

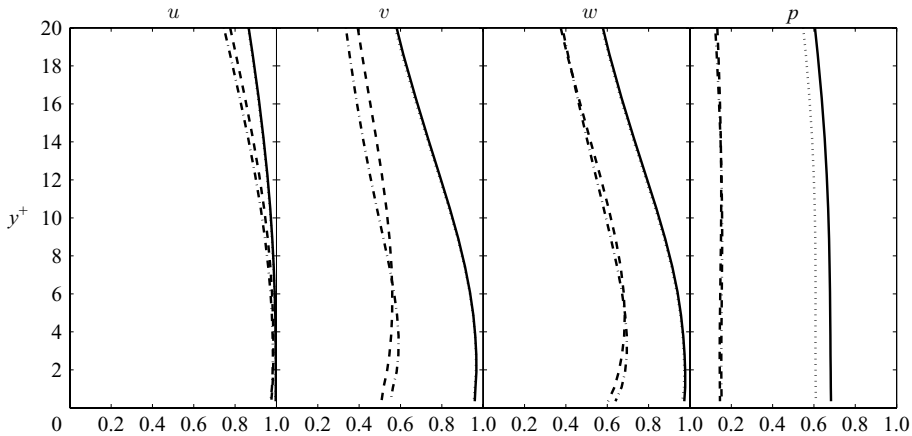


FIGURE 6. As figure 5 but ‘obtained’ using the extended the Kalman filter.

By the initialization of the estimator (based on zero knowledge of the flow-field fluctuation), the correlation is zero at $t = 0$, followed by a transient during which the correlation increases to statistically steady state. A similar transient also appears in plots of the error. Figures 5–11 report the correlations and errors as a function of y for the several cases considered at statistical steady state (that is, after the transient).

5.2. One measurement – a comparison of two stochastic models

To compare the gains based on a spatially uncorrelated stochastic model $Q = I$ with the estimation gains based on the stochastic model obtained from DNS as suggested in this study, we first compare the performance of the estimator using only the η_y measurement. This is because we only obtained a well-resolved estimation gain for the η_y measurement when using the spatially uncorrelated stochastic model.

The correlation between the real and estimated flow, for one measurement, is depicted in figure 5 and figure 6 for the Kalman and extended Kalman filters

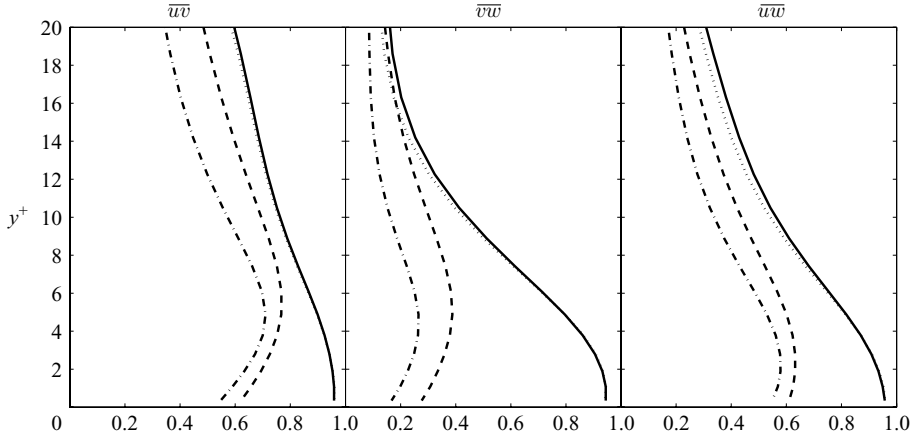


FIGURE 7. $\text{corr}_y(s, \check{s})$ for the Reynolds stresses obtained using the Kalman filter. The solid line denotes estimation using all three measurements and noise statistics as discussed in §3. The dashed line denotes the estimator performance using only the η_y measurement. The dash-dotted line is obtained using the spatially uncorrelated stochastic model for noise statistics. The dotted line denotes the estimator performance using the η_y and v_{yy} measurements.

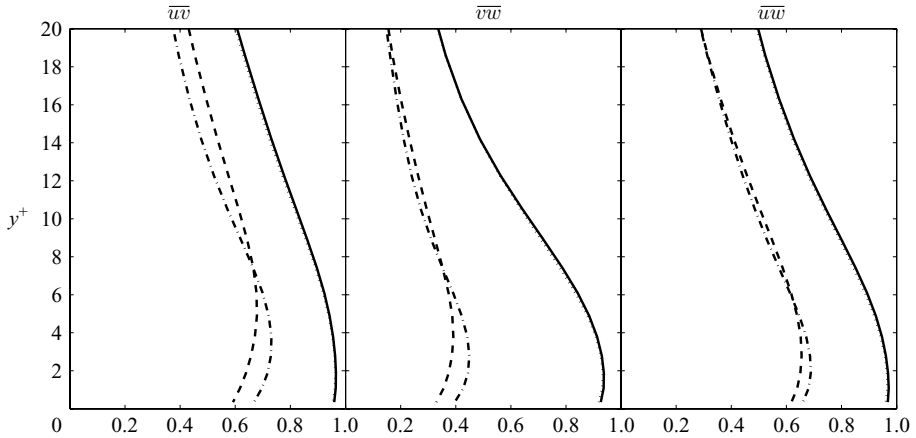


FIGURE 8. As figure 7 but obtained using the extended Kalman filter.

respectively. The dashed lines represent the stochastic model developed in this work whereas the dash-dotted lines represent the spatially uncorrelated stochastic model. The correlation for the u -component is almost 1 (perfect correlation) close to the wall for the two filters but there is an increasing difference both for the Kalman and extended Kalman filter as the wall distance increases. For v , w , and p the difference is larger. This is due to the fact that the streamwise disturbance velocity contains more energy than the other components and that with only the η_y measurement we are missing important information about the flow behaviour.

Corresponding correlations are shown in figures 7 and 8 for the Reynolds stresses $\overline{u\bar{v}}$, $\overline{v\bar{w}}$, and $\overline{u\bar{w}}$. These correlations decay faster since they depend on a squared velocity quantity. This also makes a clearer difference between the two stochastic models.

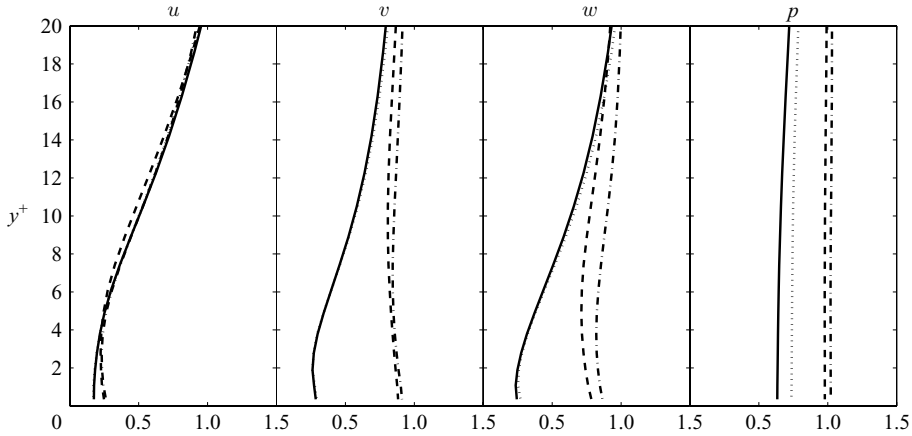


FIGURE 9. The relative estimation error $err_{n_y}(s, \check{s})$, defined as in equation (5.2) plotted for the Kalman filter. The solid line denotes estimation performed with all three measurements and gains based on turbulence statistics. The dashed line denotes the estimator performance using only the η_y measurement. The dash-dotted line is the correlation when using the spatially uncorrelated stochastic model. The dotted line denotes the estimator performance using the η_y and v_{yy} measurements.

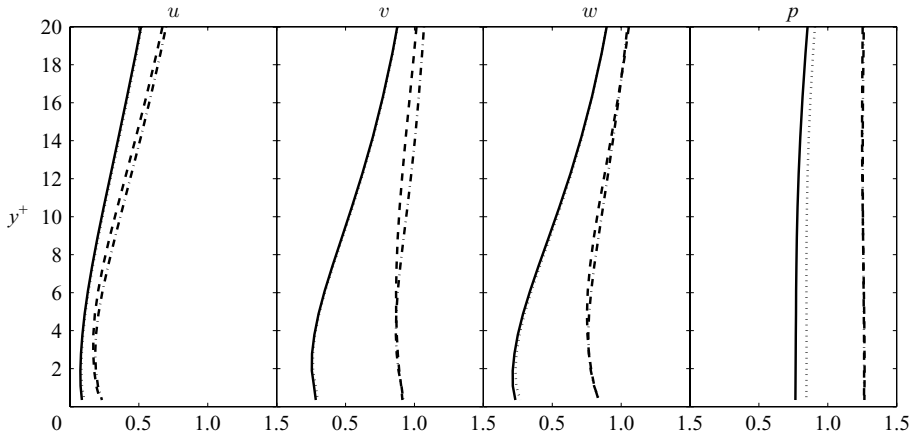


FIGURE 10. As figure 9 but plotted for the extended Kalman filter.

In figures 9 and 10 we can see similar trends for the error function (5.2) for all the primitive variables and for both the Kalman and extended Kalman filter.

For both the estimators and both stochastic models, using only the η_y gains, the correlation and error for the u -component, decay quickly beyond $y^+ \approx 8$ and in the centre region of the channel both the error and correlation measures perform poorly. The components v , w , and p are also clearly not estimated very well when only the η_y measurement is used.

5.3. Two and three measurements, using the stochastic model obtained from DNS

The performance of all three measurements combined, with the relative weighting presented in table 1, are shown as solid lines in figure 5–10.

In these figures it is clearly seen that the correlation and error between the real and estimated flow for the primitive variables and the Reynolds stresses are

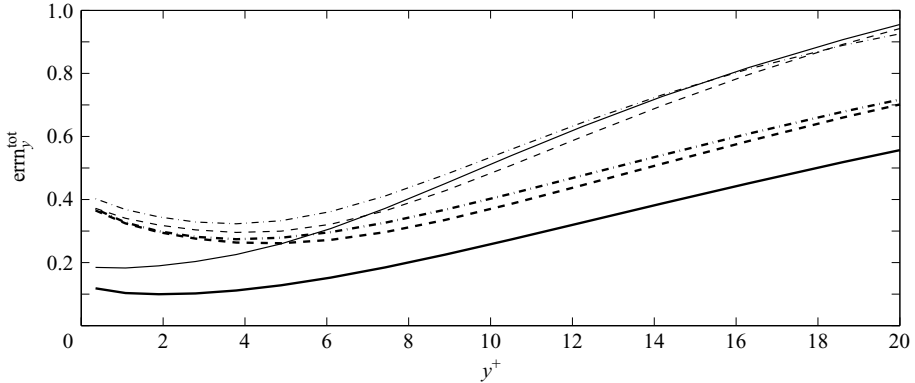


FIGURE 11. The total energy of the estimation error is shown as a function of the wall-normal distance. The solid line denotes the error when all three measurements are applied in the estimator. The dashed and dash-dotted lines represent the estimator performance when using only the η_y measurement with the stochastic model based on turbulence statistics and the spatially uncorrelated stochastic model respectively. The thick lines show the extended Kalman filter and the thin lines the Kalman filter data.

greatly improved when the additional measurements are included, as facilitated by the covariance models proposed by this study. The strongest improvement appears for the pressure, due to the addition of a pressure measurement.

The dotted lines in figure 5–10 represent the correlation when using gains based on the η_y and the v_{yy} measurements. By comparing the solid and dotted lines it is evident that the importance of the pressure measurement is relatively weak for the velocity components and the Reynolds stresses whereas for the pressure component there is a big difference. Notice also that the effect of the pressure measurement generally becomes stronger farther away from the wall.

In figure 11 the total estimation error, averaged in time, is plotted as a function of wall-normal distance. The thin lines show the Kalman filter results and the thick lines the corresponding extended Kalman filter results. The improved estimation possibilities with the stochastic model presented in this study over a spatially uncorrelated one is clearly seen in figure 11. This improvement is most pronounced close to the wall. The correlation and error for all quantities decay quickly well beyond $y^+ \approx 10$. As expected, towards the centre of the channel, by both measures, the estimator performs poorly.

The total energy of the estimation error exhibits a transient as the two simulations are started, as described in § 5.1. This transient is depicted in figure 12 for the Kalman filter simulation. Closer to the wall the transient is stronger and the error reaches a lower level than further into the flow domain. The transient is due to the fact that the estimated flow is initialized with only a turbulent mean flow profile.

In figure 13, an instantaneous plot of the v -velocity component is shown at $y^+ = 9.7$ for the flow field and the two different filters (based on three measurements). Similar structures are present in all three plots, with the extended Kalman filter visibly superior to the Kalman filter in terms of matching the actual flow.

At this time, it is impossible to compare properly the performance of the present approach to the adjoint-based estimation approach discussed in Bewley & Protas (2004), where a turbulent channel flow at $Re_\tau = 180$ was estimated based on wall measurements, as discussed in § 1.1. The difficulty is that the two methods have several adjustable parameters that are essentially incompatible (in the present strategy, the

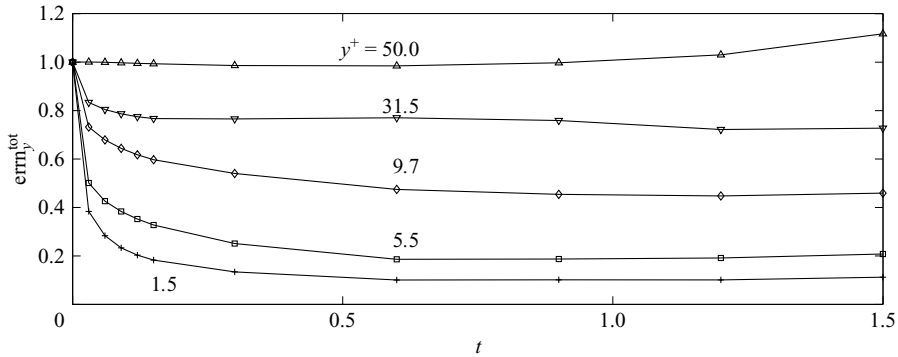


FIGURE 12. The transient of the total error energy at several values of y^+ for case 4 in table 1. All three measurements are used together with the Kalman filter; the transient exhibited by the extended Kalman filter is similar.

α parameters, and in the adjoint-based strategy, the length of the time horizon and the weighting of the so-called background term); further, these parameters, have, so far, not been adequately optimized for either approach. Thus, at this time, a proper comparison between the present extended Kalman filtering approach and adjoint-based approach proposed in Bewley & Protas (2004) to the estimation of near-wall turbulence is not possible, and remains a topic of future work.

6. Summary

A key step in framing the Kalman filter problem is the accurate statistical description of the system dynamics not fully described by the estimator model. The present paper has shown that, by determining the appropriate second-order statistical information in a full nonlinear DNS of the channel flow system, then incorporating this statistical information in the computation of the linear estimator feedback gains, an effective estimator may be built based on all three measurements available at the wall. For a given feedback amplitude, this estimator provides a better correlation between the real turbulent flow and the estimate thereof than the corresponding estimators considered for this problem in previous work. Significant improvements are obtained, as compared with estimators based on spatially uncorrelated stochastic models, in terms of both the maximum correlation near the wall and how far into the channel an adequate correlation extends. Also, the estimation gains may be transformed to physical space to obtain well-resolved convolution kernels that eventually decay exponentially with distance from the origin, thereby, ultimately, facilitating decentralized implementation.

In Part 1, the estimation of a perturbed laminar flow was investigated, and it was shown that an artificial, but physically reasonable, Gaussian distribution model for the spectral density function was adequate to obtain effective, well-behaved estimation feedback kernels for the problem of estimating the perturbed laminar flow. That result, together with the result from the present study for the problem of estimating turbulence, indicate that the choice of the disturbance model is quite significant in the effectiveness of the resulting estimator. Note that it has also been observed that a highly accurate statistical model is not essential in obtaining effective estimator performance.

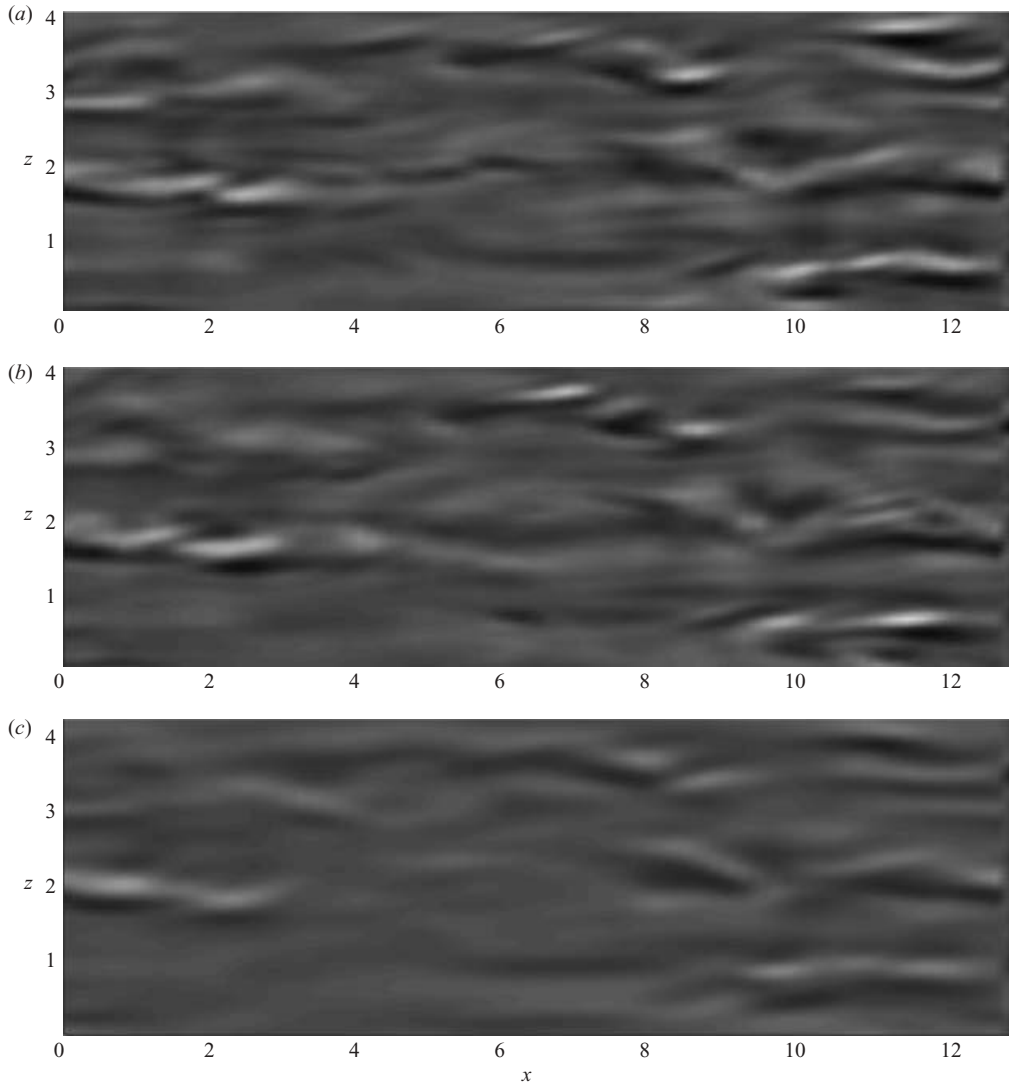


FIGURE 13. Wall-normal velocity component v plotted at $y^+ = 9.7$ at an instant in time when statistically steady state has been reached in the estimator: (a) the flow velocity itself; (b) the velocity field reproduced by the extended Kalman filter; (c) the velocity field reproduced by the Kalman filter. The contour levels range from -1 to 1 , where black and white represent the lower and upper bound respectively.

As expected, the (nonlinear) extended Kalman filter was found to outperform a (linear) Kalman filter on this nonlinear estimation problem. The estimated state in the Kalman filter deteriorates more rapidly with the distance from the wall. The extended Kalman filter captures better the structures farther into the domain, both in magnitude and phase. In terms of both correlation and estimation error, we also observed an approximate correspondence of the performance of the present extended Kalman filter with the adjoint-based estimation procedure reported in Bewley & Protas (2004). The adjoint-based approach is vastly more expensive computationally,

and, at least in theory, can account for the nonlinear dynamics of the system more accurately, so this correspondence reflects favourably on the performance of the present extended Kalman filter.

The admittedly artificial assumption of the external disturbance forcing \hat{f} being ‘white’ in time may be relaxed in future work, ‘colouring’ the noise with the time dynamics of \hat{n} , by performing a spectral factorization and augmenting the estimator model to account for the dominant time dynamics in \hat{f} . This approach, while in theory tractable for this problem, involves estimators of substantially higher dimension than the present one (which is already large), and might facilitate substantial performance improvements. Development of this approach is thus deferred for the time being as a promising area for future work on this problem.

The authors sincerely acknowledge the funding provided by the Swedish research council (VR), the Swedish Defence Research Agency (FOI), and the Dynamics and Control directorate of the Air Force Office of Scientific Research (AFOSR) in support of this work.

REFERENCES

- ANDERSON, B. & MOORE, J. 1979 *Optimal Filtering*. Prentice-Hall.
- BALAKRISHNAN, A. V. 1976 *Applied Functional Analysis*. Springer.
- BAMIEH, B., PAGANINI, F. & DAHLEH, M. A. 2002 Distributed control of spatially invariant systems. *IEEE Trans. Automatic Control* **47** (7), 1091–1107.
- BEWLEY, T. R. 2001 Flow control: new challenges for a new renaissance. *Prog. Aerospace Sci.* **37**, 21–58.
- BEWLEY, T. R. & LIU, S. 1998 Optimal and robust control and estimation of linear paths to transition. *J. Fluid Mech.* **365**, 305–349 (referred to herein as BL98).
- BEWLEY, T. R., MOIN, P. & TEMAM, R. 2001 DNS-based predictive control of turbulence: an optimal benchmark for feedback algorithms. *J. Fluid Mech.* **447**, 179–225.
- BEWLEY, T. R. & PROTAS, B. 2004 Skin friction and pressure: the “footprints” of turbulence. *Physica D* **196**, 28–44.
- FARRELL, B. F. & IOANNOU, P. J. 1996 Turbulence suppression by active control. *Phys. Fluids* **8**, 1257–1268.
- HÖPFFNER, J., CHEVALIER, M., BEWLEY, T. R. & HENNINGSON, D. S. 2005 State estimation in wall-bounded flow systems. Part 1. Perturbed laminar flows. *J. Fluid Mech.* **534**, 263–294.
- HÖGBERG, M., BEWLEY, T. R. & HENNINGSON, D. S. 2003a Linear feedback control and estimation of transition in plane channel flow. *J. Fluid Mech.* **481**, 149–175.
- HÖGBERG, M., BEWLEY, T. R. & HENNINGSON, D. S. 2003b Relaminarization of $Re_\tau = 100$ turbulence using gain scheduling and linear state-feedback control. *Phys. Fluids* **15**, 3572–3575.
- JIMENEZ, J. 1999 The physics of wall turbulence. *Physica A* **263**, 252–262.
- JOVANOVIĆ, M. R. & BAMIEH, B. 2001 Modelling flow statistics using the linearized Navier–Stokes equation. In *Proc. 40th IEEE Conf. on Decision and Control*, Orlando, FL, pp. 4944–4949.
- MOIN, P. & MOSER, R. D. 1989 Characteristic-eddy decomposition of turbulence in a channel. *J. Fluid Mech.* **200**, 471–509.
- WEIDEMAN, J. A. & REDDY, S. 2000 A MATLAB Differentiation Matrix Suite. *ACM Trans. Math. Software* **26**, 465–519.